

Comparative Analysis of Natural Ruby and Synthetic Corundum Ceramics by UV-Vis and Raman Spectroscopy

Ivan Tsanev^{*1}, Tsvetan Dimitrov², Liliya Tsvetanova¹, Rositsa Titorenkova^{1,3}

Institute of Mineralogy and Crystallography, Bulgarian Academy of Sciences, Acad. G. Bonchev Str., bl. 107, 1113 Sofia, Bulgaria¹

University of Ruse "Angel Kanchev", Razgrad Branch 7200, Bulgaria²

PERIMED, Central District, Vasil Aprilov Blvd. 15A, 4002 Plovdiv, Bulgaria³

*ivan_tsanev@imc.bas.bg

Abstract: This study presents a comparative spectroscopic investigation of natural Cr^{3+} -bearing ruby and multiphase Al_2O_3 -based ceramics derived from industrial waste. The natural corundum shows characteristic Cr^{3+} crystal-field absorption bands at ~ 405 and ~ 550 nm and sharp R-line emission near 693 nm, confirming a structurally ordered $\alpha\text{-Al}_2\text{O}_3$ lattice. In contrast, the waste-derived ceramics exhibit charge-transfer-dominated absorption associated mainly with V^{5+} and Fe^{3+} under oxidizing firing conditions. Strong UV absorption (220–300 nm) and the absence of vanadium crystal-field transitions indicate predominant V^{5+} stabilization, consistent with chemical and phase analysis. The ceramics display high lightness ($L^* \approx 93$) and a yellow hue ($b^* = 10\text{--}23$) governed by ligand-to-metal charge-transfer processes. The results demonstrate the effectiveness of combined UV-Vis and Raman spectroscopy for distinguishing crystal-field and charge-transfer mechanisms and for resolving dopant-related colour formation in alumina systems.

Keywords: $\alpha\text{-Al}_2\text{O}_3$; WASTE-DERIVED CERAMICS; VANADIUM OXIDATION STATE; CRYSTAL-FIELD TRANSITIONS; CHARGE-TRANSFER ABSORPTION; UV-VIS SPECTROSCOPY; RAMAN SPECTROSCOPY

1. Introduction

Corundum ($\alpha\text{-Al}_2\text{O}_3$) is a structurally robust and chemically stable oxide occurring both as a natural mineral and as an industrial ceramic material. Its exceptional mechanical strength, thermal resistance and chemical inertness make it essential for refractory, structural and optical applications. In its gem-quality form, ruby represents chromium-doped corundum, where Cr^{3+} substitutes for Al^{3+} in octahedral coordination, producing the characteristic red colour through spin-allowed d-d transitions and sharp $\text{R}_1\text{--}\text{R}_2$ luminescence lines near 693–694 nm. The crystal-field behaviour of Cr^{3+} in corundum has been extensively described within the framework of crystal-field theory and electronic spectroscopy [1–4].

In addition to chromium, minor transition metal ions such as Fe, Ti and V may significantly influence the optical absorption behaviour and hue of corundum. Vanadium is particularly important due to its multiple oxidation states (V^{3+} , V^{4+} , V^{5+}), each associated with distinct electronic and charge-transfer transitions. In natural systems, V^{3+} may contribute to absorption in the UV-blue region, whereas V^{4+} and especially V^{5+} are commonly linked to broad $\text{O}^{2-} \rightarrow \text{V}$ charge-transfer bands that modify colour saturation and absorption edge characteristics [5–7,10].

Natural Cr^{3+} -bearing corundum from the village of Mishevsko (Eastern Rhodopes, Bulgaria) was recently characterized using UV-Vis, Raman and photoluminescence spectroscopy [1]. The study revealed well-resolved Cr^{3+} absorption bands at ~ 405 and ~ 550 nm, sharp $\text{R}_1\text{--}\text{R}_2$ emission lines, and additional absorption features in the UV-blue region attributed to minor V and Ti admixtures. These results define a structurally ordered $\alpha\text{-Al}_2\text{O}_3$ reference system in which chromium is the principal chromophore and vanadium acts as a secondary modifier of the optical response.

In contrast, Al_2O_3 -based ceramics derived from industrial waste represent chemically complex multicomponent systems containing vanadium, iron, alkali elements and silica-rich phases. During high-temperature processing in an oxidizing atmosphere, vanadium is predominantly stabilized as V^{5+} , favouring intense ligand-to-metal charge-transfer transitions in the UV region. Moreover, the coexistence of multiple crystalline polymorphs of Al_2O_3 (α - and κ -phases), together with cristobalite (SiO_2) and residual amorphous material, results in heterogeneous optical behaviour governed by both crystal-field and charge-transfer mechanisms.

Consequently, colour formation in such engineered ceramics cannot be interpreted solely within the classical crystal-field framework typical of ruby, but must also consider oxidation-state equilibria, phase interactions and defect chemistry.

UV-Vis diffuse reflectance spectroscopy provides information on electronic transitions and oxidation states of transition metal ions, whereas Raman spectroscopy offers a structural fingerprint of $\alpha\text{-Al}_2\text{O}_3$ and related ceramic phases, as well as luminescent signatures of Cr^{3+} and other dopants [3,8]. The combination of these techniques enables differentiation between Cr^{3+} -controlled crystal-field coloration and vanadium- or iron-dominated charge-transfer absorption in complex Al_2O_3 -based systems.

The present study presents a comparative spectroscopic investigation of a natural Cr^{3+} -bearing ruby [1] and synthetic Al_2O_3 -based multiphase ceramics derived from industrial waste containing a wide range of impurities, including vanadium and iron. The objective is to correlate dopant chemistry and oxidation state with UV-Vis absorption behaviour, Raman structural features and Cr^{3+} luminescence characteristics, as well as CIELAB colour coordinates. By comparing a structurally ordered natural $\alpha\text{-Al}_2\text{O}_3$ reference with chemically complex waste-derived ceramics, the study highlights the capability of combined UV-Vis and Raman spectroscopy to distinguish crystal-field and charge-transfer mechanisms, detect oxidation-state variations, and resolve subtle differences in dopant environment and lattice structure.

2. Materials and Methods

2.1 Samples

Ruby: Natural corundum containing Cr^{3+} and traces $\text{V}^{3+}/\text{V}^{4+}$ and other transition metal ions (after Ref. [1]).



Sample-00 2.7x2.9x3.5 mm



Sample-04 1.8x2.0x2.3 mm



Sample-07 1.1x2.0x2.3 mm



Sample-09 1.5x1.6x1.8 mm

Figure. 1 Vanadium-bearing natural ruby crystals from the Eastern Rhodopes (Bulgaria). The colour variations reflect minor vanadium incorporation in Cr^{3+} -doped $\alpha\text{-Al}_2\text{O}_3$, where vanadium acts as a secondary chromophore modifying the UV-blue absorption region.

Synthetic ceramic: The spent catalyst with a complex chemical and phase composition is mixed with chemically pure reagents (Al_2O_3) for the production of multiphase ceramics by one-step solid-phase sintering method. The mixture was homogenized and sintered in a laboratory muffle furnace with a heating rate $500^\circ\text{C}/\text{h}$ in air with isothermal retention of 2 h at the final temperatures of 1200°C and 1300°C .

2.2 Analytical methods

Phase composition was analysed using a Bruker D8 Advance and Empyrean (Malvern Panalytical) powder X-ray diffractometers with $\text{Cu K}\alpha$ radiation operating at 40 kV and 30 mA, in the range $10 - 80^\circ 2\theta$. Pulse height distribution (PHD) optimization procedures have been applied in order to reduce the fluorescence-induced background and peak-to-background ratio.

Wavelength Dispersive X-ray Fluorescence Spectroscopy (WDXRF) was used to determine the chemical composition using Supermini 200 (Rigaku, Japan) spectrometer operating at 50 kV and 4.00 mA. The powder samples were pressed to obtain a tablet. The weight ratio of the amount of sample to the amount of glue (Acrawax C powder) was 5:1. A semi-quantitative method (SQX) was used to determine the elemental composition.

Diffuse reflectance spectra were recorded using a Cary 4000 (Agilent) UV-Vis spectrophotometer equipped with an internal DRA 900 integrating sphere accessory. Measurements were performed in the $200\text{--}800$ nm spectral range with a spectral resolution of 1 nm. The reflectance data were baseline-corrected and transformed using the Kubelka-Munk function $F(R)$ to obtain absorption-related spectra suitable for comparison with the natural corundum reference. UV-Vis transmittance spectra of the natural ruby samples were collected in the same spectral range using a solid-sample transmission accessory.

Raman spectra and photoluminescence (PL) measurements were performed using a WiTec alpha300 R confocal Raman microscope with a 532 nm laser and $\times 50$ objective, producing a laser spot of $\sim 1 \mu\text{m}$. Each PL spectrum was recorded with an acquisition time of 0.05 s and averaged over 20 accumulations.

The colour of the ceramics was measured using a Lovibond Tintometer RT 100 and presented in the CIELAB colour space.

3. Results and Discussion

3.1. Phase composition of the studied samples

Rubies samples consist $\alpha\text{-Al}_2\text{O}_3$ with trace Ti, V, Cr and Fe [1].

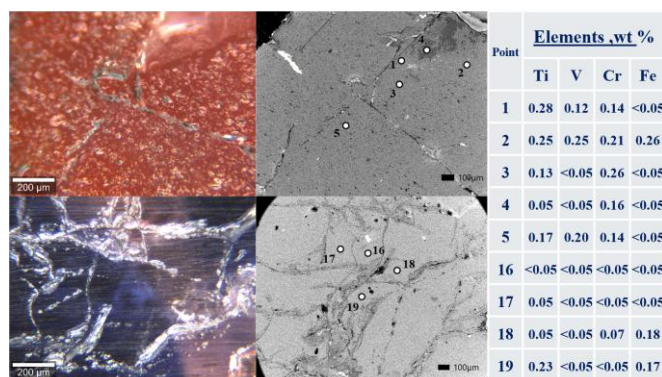


Figure 2. X-ray diffraction pattern of the natural ruby (after Ref. [1]) confirming single-phase $\alpha\text{-Al}_2\text{O}_3$ with trace substitution of transition metal ions (Cr, V, Ti, Fe) in the corundum lattice.

Synthetic ceramics were obtained from industrial waste with the following composition: SiO_2 (55.7 wt %), SO_3 (22.8 wt %), K_2O (11.95 wt %), V_2O_5 (4.36 wt %), Al_2O_3 (2.32 wt %), Na_2O (1.47 wt %), Fe_2O_3 (0.81 wt %), CaO (0.36 wt %), Cs_2O (0.13 wt %), As_2O_3 (0.1 wt %), P_2O_5 (0.05 wt %) and others (0.14 wt %) and addition of Al_2O_3 in an amount necessary to obtain a 1.5 molar ratio of

$\text{Al}_2\text{O}_3/\text{SiO}_2$. 100g waste+140 g Al_2O_3 . The mixture was homogenized and sintered in a laboratory muffle furnace with a heating rate of $200^\circ\text{C}/\text{h}$ in an air atmosphere with an isothermal retention of 2 h at final temperatures of 1200°C and 1300°C .

The phase composition of the resulting ceramic sintered at 1100°C , 1200°C , and 1300°C determined based on the X-ray diffraction patterns (Figure 3), is presented in Table 1.

Table 1. Quantitative phase composition (wt.%) of ceramics sintered at different temperatures, determined from XRD data.

Sample	$\alpha\text{-Al}_2\text{O}_3$	$\kappa\text{-Al}_2\text{O}_3$	cristobalite	amorphous
1100°C	55%	21%	24%	28%
1200°C	56%	30%	14%	23%
1300°C	43%	42%	16%	26%

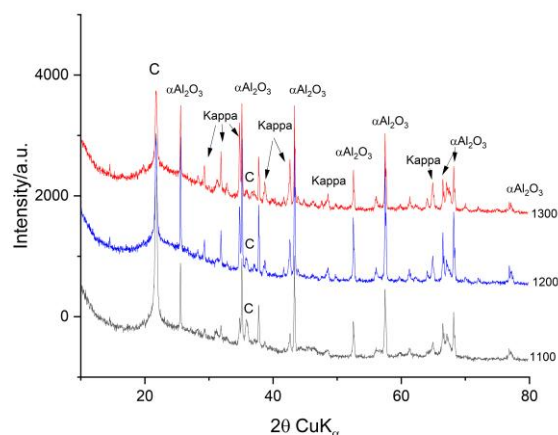


Figure 3. X-ray diffraction patterns of waste-derived ceramics sintered at 1100°C , 1200°C and 1300°C . Indexed reflections of $\alpha\text{-Al}_2\text{O}_3$, $\kappa\text{-Al}_2\text{O}_3$ and cristobalite illustrate temperature-dependent phase evolution under oxidizing firing conditions.

3.2. Chemical composition (XRF data)

The chemical composition of the ceramic sintered at 1100°C , 1200°C , and 1300°C expressed as weight percent oxides, is present in Table 2.

Table 2. Chemical composition of the sintered ceramics.

Oxides, wt%	1100°C	1200°C	1300°C
Na_2O	0.83	1.06	1.03
Al_2O_3	46.2	41.6	40.5
SiO_2	41.4	44.4	45.6
P_2O_5	0.022	0.02	-
SO_3	0.25	0.25	0.06
Cl	0.01	-	-
K_2O	6.41	7.35	7.6
CaO	0.18	0.18	0.21
TiO_2	0.08	0.12	-
V_2O_5	3.70	4.13	4.1
Fe_2O_3	0.85	0.90	0.93
CuO	0.021	0.02	0.03
As_2O_3	0.073	0.05	0.03
MoO_3	-	0.02	0.02

3.3. Optical absorption spectra

Natural ruby: The UV-Vis spectrum of the natural ruby exhibits well-resolved spin-allowed d-d transitions of Cr^{3+} centred at ~ 550 nm, together with higher-energy bands near 405 nm (Fig. 4). Weak absorption features in the 400 and 600 nm region indicate minor contributions from $\text{V}^{3+}/\text{V}^{4+}$, while an increase in absorption below 320 nm is attributed to ligand-to-metal charge-transfer transitions involving trace V^{5+} . The sharp R-line emission at ~ 693 nm confirms the presence of structurally ordered Cr^{3+} in the $\alpha\text{-Al}_2\text{O}_3$ lattice [1,4,9].

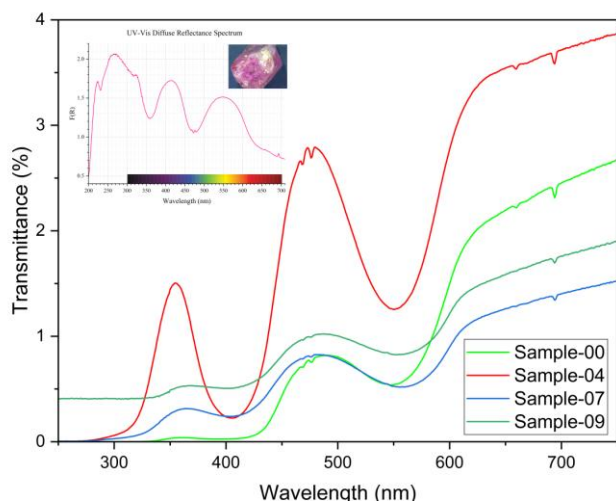


Figure 4. UV-Vis transmittance spectra of vanadium-bearing natural ruby samples showing characteristic Cr^{3+} crystal-field absorption bands at ~ 405 and ~ 550 nm together with enhanced UV-blue attenuation (below ~ 320 – 400 nm) attributed to $\text{V}^{3+}/\text{V}^{4+}$ crystal-field transitions and $\text{O}^{2-} \rightarrow \text{V}^{5+}$ charge-transfer processes. The spectra demonstrate the role of vanadium as a secondary chromophore modifying the absorption edge [5–7,9].

Synthetic corundum ceramic: In contrast, the synthetic ceramics exhibit strong and broad absorption in the 220–300 nm range, characteristic of $\text{O}^{2-} \rightarrow \text{V}^{5+}$ charge-transfer transitions (Fig.5). Crystal-field d–d transitions of vanadium are largely suppressed, indicating that vanadium is predominantly stabilized in its highest oxidation state under oxidizing firing conditions. A weak band near ~ 700 nm may suggest minor V^{4+} species associated with oxygen-deficient sites.

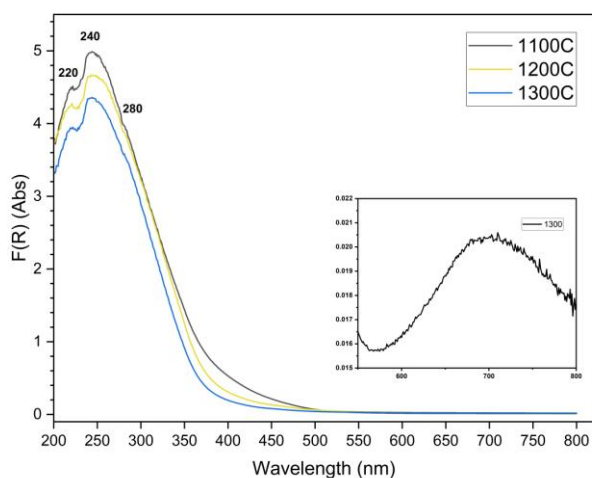


Figure 5. UV-Vis diffuse reflectance spectra of waste-derived alumina ceramics showing dominant $\text{O}^{2-} \rightarrow \text{V}^{5+}$ charge-transfer absorption in the 220–300 nm region and broad visible absorption associated with Fe^{3+} species, confirming charge-transfer-controlled colour formation [5–7].

The visible region is dominated by broad overlapping absorption features attributed to Fe^{3+} and vanadium-related charge-transfer processes. The absence of distinct Cr^{3+} -type transitions confirms a fundamentally different chromophore mechanism compared to natural ruby.

When Al_2O_3 reacts with vanadium-containing species in air atmosphere, the formation of AlVO_4 is thermodynamically favoured, further supporting stabilization of V^{5+} . This interpretation is consistent with XRF data showing significant V_2O_5 content and with the observed yellow colour coordinates.

3.4 Raman Spectroscopy

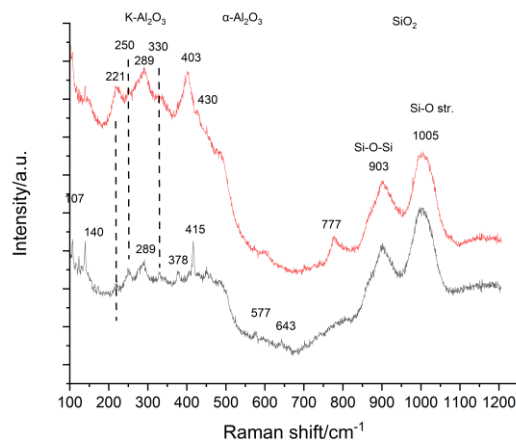


Figure 6. Raman spectra of waste-derived ceramics illustrating vibrational modes of $\alpha\text{-Al}_2\text{O}_3$, $\kappa\text{-Al}_2\text{O}_3$, cristobalite and amorphous silica, confirming the multiphase structure of the sintered system.

The natural ruby crystallizes in the trigonal $\alpha\text{-Al}_2\text{O}_3$ structure (space group $R\bar{3}c$), where Cr^{3+} substitutes for Al^{3+} in octahedral coordination without symmetry modification. Group theoretical analysis predicts seven Raman-active modes, and experimentally well-defined bands at 378, 415, 430, 577 and 643 cm^{-1} confirm a structurally ordered corundum lattice [3,4].

In contrast, the Raman spectra of the synthetic ceramics reveal multiphase composition. The presence of $\kappa\text{-Al}_2\text{O}_3$ (orthorhombic polymorph) introduces additional vibrational modes due to its lower symmetry and multiple non-equivalent Al sites, producing bands near ~ 250 , 300 and 500 cm^{-1} . Cristobalite contributes intense peaks at ~ 500 and 770 cm^{-1} , while the amorphous phase is characterized by broad bands in the 900 – 1100 cm^{-1} region (Fig.6) [8].

Under 532 nm excitation, luminescence lines associated with Cr^{3+} electronic transitions are also observed, indicating trace chromium incorporation despite the absence of ruby-type colouration (Fig. 7) [1,4,9].

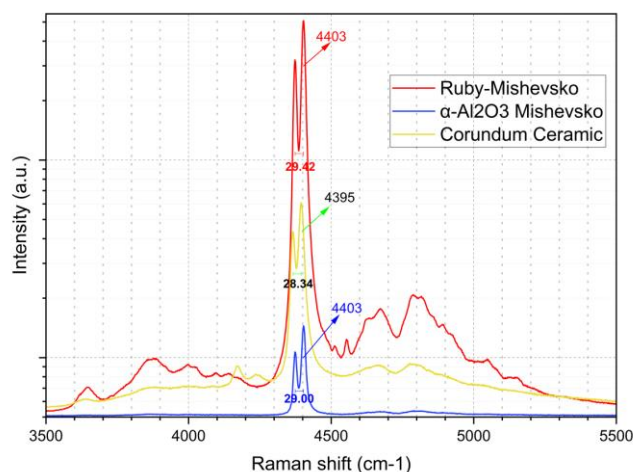


Figure 7. Raman spectra of natural ruby and synthetic ceramic under 532 nm excitation showing Cr^{3+} R_1 and R_2 luminescence lines. The R_1 peak is positioned at 4403 cm^{-1} Raman shift for natural ruby and 4395 cm^{-1} Raman shift for the synthetic ceramic, indicating lattice strain and structural differences.

The R_2 – R_1 separation equals 29.00 cm^{-1} for weakly luminescent natural corundum, 29.42 cm^{-1} for strongly luminescent natural corundum ($\approx 30\times$ higher intensity), and 28.34 cm^{-1} for the ceramic.

Variations in peak position and splitting reflect differences in crystal-field strength, dopant environment and structural order between the natural α -Al₂O₃ reference and the multiphase waste-derived ceramic.


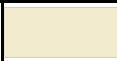
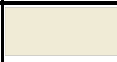
3.5. Colour

The optical neutrality of pure Al₂O₃ implies that colour in both systems originates exclusively from transition metal ions.

In ruby, the red colour arises from spin-allowed d–d transitions of Cr³⁺ in octahedral coordination, which selectively absorb blue and green light, resulting in red transmission and characteristic emission near 696 nm [2–4].

In the synthetic ceramics, however, the colour is yellow despite the presence of Cr³⁺ luminescence. CIELAB measurements show high lightness ($L^* \approx 92$ –93), negligible red–green contribution ($a^* \approx -1$), and pronounced yellow component ($b^* = 10$ –23) [12].

Table 3. CIELAB colour coordinates (L^* , a^* , b^*) of waste-derived ceramics.

Composition	T, °C	Colour	L^*	a^*	b^*
Ceramics: α -Al ₂ O ₃ , κ -Al ₂ O ₃ , cristobalite, amorphous	1100		92.2	-1.0	23.4
	1200		93.1	-1.0	15.0
	1300		93.2	-1.1	10.5

The high lightness is explained by the dominance of colourless high-band-gap phases (α -Al₂O₃, κ -Al₂O₃, cristobalite and amorphous silica) which efficiently scatter light. The yellow hue originates primarily from ligand-to-metal charge-transfer absorption of V⁵⁺ and Fe³⁺ in the blue spectral region. The absence of positive a^* values confirms that Fe³⁺ does not induce significant red coloration under the studied conditions [5-7,10,12].

4. Conclusion

This comparative study demonstrates that colour formation in alumina systems is governed by fundamentally different electronic mechanisms in natural and waste-derived materials.

In natural ruby, colour is controlled by Cr³⁺ crystal-field transitions within a structurally ordered α -Al₂O₃ lattice [2–4]. In contrast, the engineered multiphase ceramics exhibit charge-transfer-dominated absorption, primarily associated with V⁵⁺ and Fe³⁺ stabilized under oxidizing firing conditions [5–7,10].

The shift of the Cr³⁺ R₁ line (4403 → 4395 cm⁻¹) and variations in R-line splitting (29.42–28.34 cm⁻¹) confirm structural and crystal-field differences between natural and synthetic systems [1,4,9].

Vanadium oxidation-state stabilization emerges as a key technological parameter controlling optical response in alumina ceramics derived from secondary raw materials. The combined use of UV–Vis and Raman spectroscopy provides a reliable diagnostic tool for oxidation-state monitoring, phase verification and targeted colour engineering under sustainable processing conditions [3,8,11].

Industrial Relevance Statement

Control of vanadium oxidation state and phase composition enables predictable colour tuning in waste-derived alumina ceramics, supporting sustainable valorisation of industrial residues into functional ceramic materials.

Acknowledgements:

The financial support of this work by the Bulgarian Ministry of Education and Science, National Research Fund under the contract number KP-06-H87/14 - 2024 is gratefully acknowledged.

This work also has been carried out in the framework of the National Science Program "Critical and strategic raw materials for a green transition and sustainable development", approved by the Resolution of the Council of Ministers № 508/18.07.2024 and funded by the Ministry of Education and Science (MES) of Bulgaria.

We would like to express our gratitude for the analytical support to programme "Research, Innovation and Digitalisation for Smart Transformation" 2021–2027, funded by the European Union, Project BG16RFPR002-1.014-0007 "Center for Competence PERIMED-2".

References

1. I. Tsanev et al., Rev. Bulg. Geol. Soc. **86(2)**, 54–58 (2025)
2. R.G. Burns, *Mineralogical Applications of Crystal Field Theory*, Cambridge University Press, Cambridge (1993)
3. D.S. McClure, *J. Chem. Phys.* **36**, 2757–2779 (1962)
4. S.P.S. Porto, R.S. Krishnan, *J. Chem. Phys.* **47**, 1009–1012 (1967)
5. B.J. Reddy, L.R. Moorthy, *Pramana J. Phys.* **19**, 449–454 (1982)
6. H.H. Tippins, *Phys. Rev. B* **1**, 126–135 (1970)
7. J. Ferguson, P.E. Fielding, *Chem. Phys. Lett.* **10**, 262–265 (1971)
8. E.V. Dubinsky et al., *Gems Gemol.* **56**, 2–28 (2020)
9. D. Bersani, P.P. Lottici, *Anal. Bioanal. Chem.* **397**, 2631–2646 (2010)
10. E. Fritsch, G.R. Rossman, *Gems Gemol.* **24**, 3–15 (1988)
11. P. Kubelka, F. Munk, *Z. Tech. Phys.* **12**, 593–601 (1931)
12. ISO/CIE 11664-4:2019, *Colorimetry – Part 4: CIE 1976 L*a*b* colour space* (International Organization for Standardization, Geneva, 2019)